J Solid State Electrochem (2003) 7: 348–354
DOI 10.1007/s10008-002-0337-9

ORIGINAL PAPER

T.S. Zhang · L.B. Kong · Z.Q. Zeng · H.T. Huang
P. Hing · Z.T. Xia · J. Kilner

Sintering behavior and ionic conductivity of $Ce_{0.8}Gd_{0.2}O_{1.9}$ with a small amount of MnO_2 doping

Received: 9 April 2002 / Accepted: 9 October 2002 / Published online: 27 November 2002

Abstract A 20% $GdO_{1.5}$ doped ceria solid solution with a small amount of MnO_2 doping (≤ 5% molar ratio) was prepared via the mixed oxide method from high-purity commercial powders with grain size around 0.2–0.5 μm. X-ray diffraction analysis indicated that all the samples exhibited the fluorite structure, and no new phase was found. The data from dilatometeric measurements and scanning electron microscopy observations revealed that 1% Mn doping reduced the sintering temperature by over 150 °C, and enhanced the densification and grain growth. Mn doping has little effect on grain interior conductivity, but a marked deterioration in grain boundary behavior is observed. This leads to a lower total conductivity in comparison with the undoped $Ce_{0.8}Gd_{0.2}O_{2-\delta}$. Therefore, for solid oxide fuel cells (SOFCs) with Mn-containing compounds as electrodes, optimization of electrode fabrication conditions is needed to prevent the formation of a lower conductivity layer at the electrode/electrolyte interface since Mn will diffuse from the electrode side to the electrolyte during fabrication and operation of SOFCs.

Keywords Ceria · Ceria-based solid solution · Gadolinia · Manganese oxide · Solid oxide fuel cell

T.S. Zhang (✉) · L.B. Kong · Z.Q. Zeng · H.T. Huang · P. Hing
Advanced Materials Research Centre,
School of Materials Engineering,
Nanyang Technological University,
Nanyang Avenue, Singapore 639798
E-mail: maszt@nus.edu.sg
Fax: +65-790-0920

Z.T. Xia
School of Mechanical and Production Engineering,
Nanyang Technological University,
Nanyang Avenue, Singapore 639798

J. Kilner
Department of Materials, Imperial College of Science,
Technology and Medicine, London, SW7 2AZ, UK

Introduction

Yttria-stabilized zirconia (YSZ) is generally used as an electrolyte material for the solid oxide fuel cell (SOFC) because of its good mechanical strength and high stability under oxidizing and reducing atmospheres at high temperatures [1, 2]. The YSZ electrolyte usually has to be operated at about 1000 °C, where the ionic conductivity reaches the required high level. However, such high temperatures often lead to a high fabrication cost and degradation of cell components, as well as to low efficiency of the fuel cell.

To reduce the operating temperature of the SOFC system, much attention has been paid recently to doped CeO_2-based materials, especially to the solid solution $(CeO_2)_{0.8}(Gd_2O_3)_{0.1}$, which is considered to be one of the most promising candidates for reduced-temperature SOFC systems [3, 4, 5]. However, one of the main drawbacks of CeO_2-based materials is that they are difficult to densify below 1500 °C [6, 7]. In order to reduce sintering temperatures, most of the investigators use ultrafine CeO_2-based powders, which are prepared by chemical and physical methods [7, 8, 9]. For large-scale industrial fabrication, however, it is useful to improve the sinterability of commercial powders by using sintering promoters. Some transition metal oxides, such as MnO_2, Fe_2O_3, Co_3O_4 and CuO, have been proven to be effective sintering aids for the densification of ceria-based powders [10, 11, 12]. It seems that Co_3O_4 and CuO are the most effective in promoting the densification of nano-sized ceria powders [11]. As observed by Kleinlogel and Gauckler [11], however, exceeding the temperature at which 98% density is observed (i.e., ~1100 °C for CuO and ~ 1250 °C for Co_3O_4) leads to oversintering and expansion of the doped samples. This is due to the lower melting point of these two dopants, as well as the solubility between the solid and the liquid. It is well known that extensive densification during liquid sintering is observed with a high solid solubility in the liquid, while a low solid solubility in the liquid coupled

to a high solubility of the liquid in the solid gives swelling. It is obvious that the doping effect of Co_3O_4 or CuO belongs to the latter case. Therefore, Co_3O_4 and CuO are not suitable as sintering aids for the densification of ceria-based powders with larger grain sizes (e.g., >0.1 μm), because a higher sintering temperature (usually >1300 °C) is needed to obtain a higher density. This is why Kovalevskii et al. [13] obtained only 95% of the theoretical density for the composition $Ce_{0.9-x}Co_xGd_{10}O_{2-\delta}$ ($x=0$–0.30) sintered at 1470 °C for over 5 h.

In our previous work [14, 15], MnO_2 and Fe_2O_3 have been proven to be more effective sintering aids for ceria powders with a large grain size (>0.1 μm). The present work is aimed at studying the effect of MnO_2 doping on the sintering behavior and ionic conductivity of $Ce_{0.8}Gd_{0.2}O_{1.9}$ prepared by the conventional mixed oxide method.

Experimental

Sample preparation

Mixtures of ceria, gadolinia and dopant with a Ce:Gd:Mn atomic ratio of $(80-x):20:x$ ($0 \le x \le 5$) were prepared by the conventional mixed oxide method from high purity ($>99.9\%$) commercial powders. All these raw powders exhibit almost the same grain size ($\sim$0.2–0.5 μm) according to scanning electron microscopy (SEM) observations. The mixtures were ground in ethanol by ball milling for over 24 h and dried, then pressed at 100 MPa into pellets using a die 10 mm in diameter. The green densities are about 60% of theoretical. The samples were sintered in a furnace at 1200–1700 °C for 5 h in air. Some sintering experiments were performed in a dilatometer (Setsys 16/18, Setaram, France).

Sample characterization

The crystal phases were identified by X-ray diffraction. The microstructure evolution was observed by SEM. The average grain size was calculated using the linear intercept method by counting more than 250 grains from SEM micrographs. After the pellets were sintered at 1300–1700 °C for 5 h in air and polished with emery paper, silver wires were used as the electrodes and silver paste at 850 °C was used to fix silver wire onto both sides of the sintered pellets. The ionic conductivity was measured over 200–850 °C in air using impedance spectroscopy (Gamry PC-750, USA) in the frequency ranging from 0.001 Hz to 100 kHz.

Results and discussion

Figure 1 shows the linear shrinkage rate as a function of temperature for the samples with different Mn contents. It can be seen that with increasing Mn content there is a decrease in the temperature of maximum shrinkage rate (T_{max}). For example, a decrease from 1516 °C for $(CeO_2)_{0.8}(Gd_2O_3)_{0.1}$ to 1345 °C for $(CeO_2)_{0.79}(Gd_2O_3)_{0.1}Mn_{0.01}$ is observed. This suggests that 1% Mn doping reduces the sintering temperature by over 150 °C. However, when the dopant content is greater than 1%, no significant shift of T_{max} towards the low-temperature region can be observed.

Isothermal sintering behavior for undoped and 1% Mn-doped samples was evaluated from dilatometeric measurements at a heating rate of 15 K/min. The results are shown in Fig. 2. For the 1% Mn-doped sample, at 1350 °C the relative density (RD) is $\sim$95% after 2 h, and at 1450 °C after 2 h over 98% RD can be reached. For the sample without Mn doping, at 1500 °C after 2 h only about 95% RD can be obtained. In order to obtain a sample with over 98% RD, the sintering temperature must be over 1550 °C.

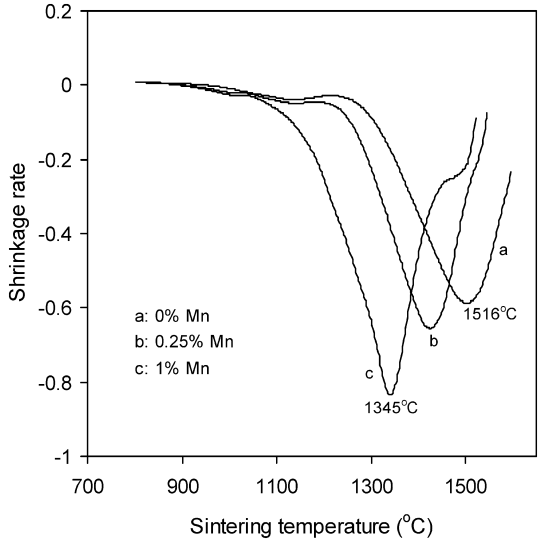

Fig. 1 Shrinkage rate against sintering temperature at a heating rate of 10 °C/min for (*a*) 0%, (*b*) 0.25% and (*c*) 1% Mn-doped $Ce_{0.8}Gd_{0.2}O_{1.9}$

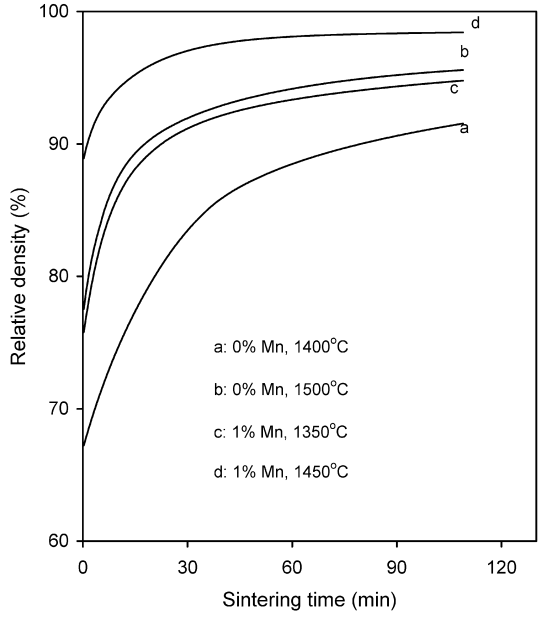

Fig. 2 Effect of sintering time and temperature on density of undoped and 1% Mn-doped $Ce_{0.8}Gd_{0.2}O_{1.9}$

Selected microstructures of undoped and 1% Mn-doped samples sintered at 1300 °C and 1500 °C are shown in Fig. 3. The undoped sample sintered at 1300 °C for 5 h, as shown in Fig. 3A, is very porous (only ~82% RD). Pores exist in the form of continuous open porosity and no obvious grain growth can be observed. Under the same sintering condition, however, the 1% Mn-doped sample (Fig. 3C) has ~95% RD. Pores are closed and isolated, and grain growth has taken place. In some regions shown in Fig. 3C there exist some larger grains, indicating inhomogeneity of Gd distribution because gadolinia has a tendency to depress the grain growth of CeO_2 [16]. These larger grains usually contain a small amount of gadolinia. In addition, only one type of pore close to large grains can be identified. These pores and large grains will disappear with increasing sintering temperatures. As shown in Fig. 3D, the 1% Mn-doped sample sintered at 1500 °C is much denser (>98.0% RD) and exhibits a uniform grain size distribution. For the undoped samples, as the sintering temperature increases from 1200 °C to 1700 °C the microstructure develops in a similar way to that of the 1% Mn-doped sample, although the temperatures needed for microstructure evolution of the undoped samples are elevated by over 100–200 °C. This can be easily shown by comparing the micrographs of Fig. 3A and B with those of Fig. 3C and D.

Fig. 3 SEM micrographs of undoped samples sintered at **A** 1300 °C and **B** 1500 °C, and 1% Mn-doped samples sintered at **C** 1300 °C and **D** 1500 °C for 5 h

Figure 4 shows the effect of sintering temperature on the sintered density and grain size of the undoped and 1% Mn-doped samples. It can be seen that the densification and the onset of grain growth for the undoped samples are delayed by over 150 °C compared with those of the 1% Mn-doped samples. For example, the 1% Mn-doped samples sintered at 1400 °C have ~97.7% RD and ~1.60 μm (in grain size), while the undoped samples sintered at 1550 °C have only ~96.8% RD and ~1.56 μm (in grain size). It is also noted that the grain size of the 1% Mn-doped samples increases from ~1.60 μm at 1400 °C to ~30.5 μm at 1550 °C, but only to ~1.56 μm at 1550 °C and ~7.8 μm at 1700 °C for undoped samples.

Inspection of Figs. 1, 2, 3, 4 indicates that small amount of Mn doping leads to a strong effect on densification, microstructure and grain growth of ceria-based solid solutions. This may result from different sintering mechanisms for undoped and Mn-doped samples. Kleinlogel and Gauckler [11] found that some transition metal oxides (TMO), such as MnO_2, Fe_2O_3, Co_3O_4 and CuO, could strongly enhance the densification of ceria powders. They speculated that the liquid-phase sintering dominated the densification behavior of Co-doped ceria solutions, because they observed a thin amorphous cobalt oxide film within grain boundary under transmission electron microscopy (TEM). Lewis et al. [12] attributed the enhanced densification to the conversion of Co_3O_4 to CoO, because they observed this conversion temperature close to the value of T_{max}

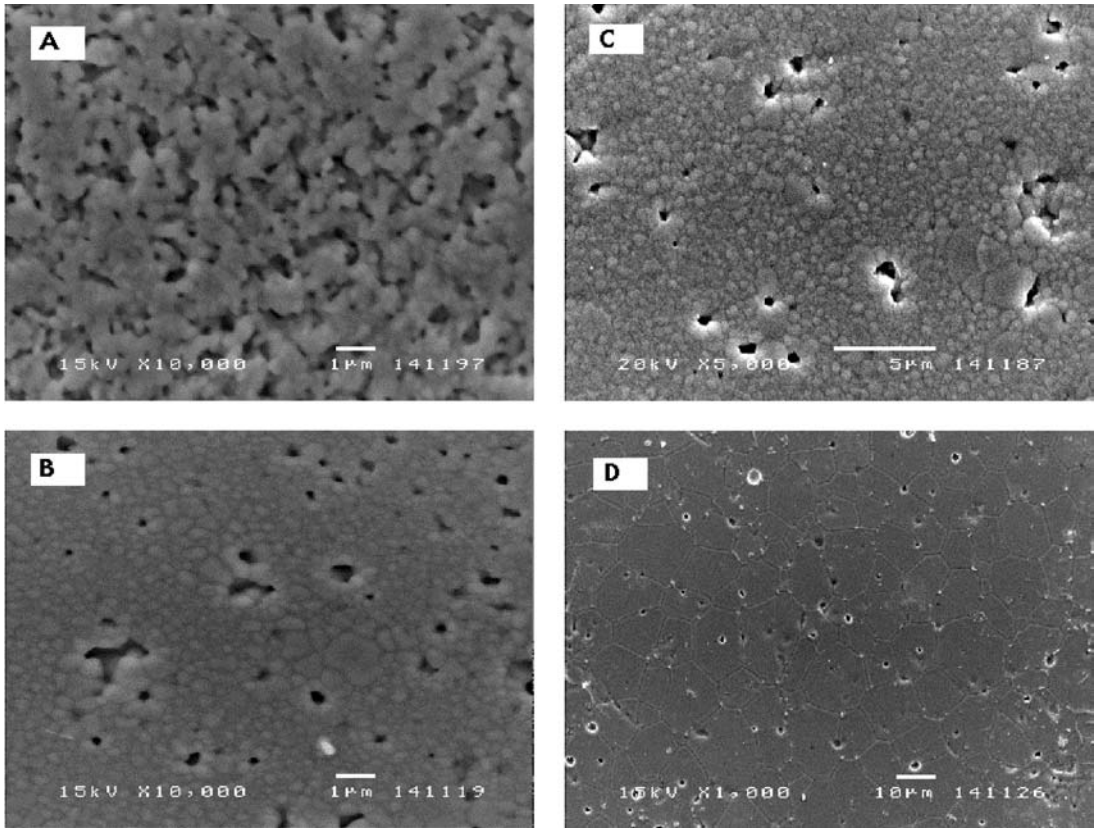

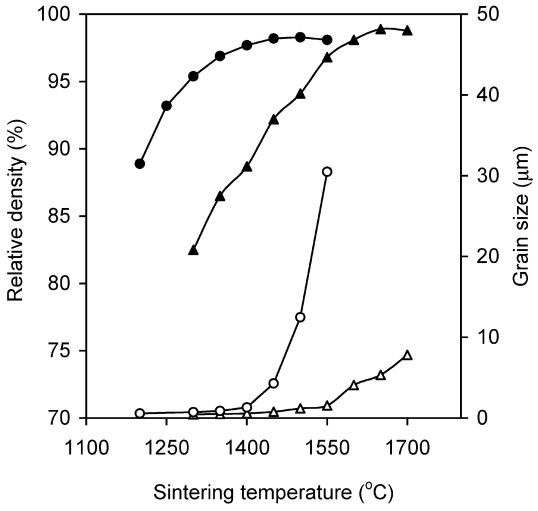

Fig. 4 Effect of sintering temperature on density and grain size of undoped samples (*filled and open triangles*) and 1% Mn-doped samples (*filled and open circles*); holding time: 5 h

(~900 °C), although they also observed an amorphous phase existing in the grain boundary. It is evident that the above explanations are full of contradictions, and do not reasonably account for the enhanced densification of Co-doped ceria for the following reasons. (1) The observed amorphous phase within the grain boundary does not provide enough evidence for the existence of a liquid phase. It is well known that the melting point of cobalt oxides is over 1250 °C; however, the enhanced densification temperature (T_{max}) occurred at ~900 °C. It is impossible for the appearance of a liquid phase at this temperature. (2) In addition, no evidence from phase diagram or thermal gravimetric and differential thermal analysis reveals the existence of liquid phases between ceria and cobalt oxide below 1300 °C.

It is interesting to note that these TMOs (i.e., MnO_2, Fe_2O_3, CoO and CuO) have been found to be effective sintering aids for the densification of some metal oxides [10, 17, 18, 19, 20], such as SnO_2, CeO_2, TiO_2 and ZrO_2. Various explanations of the enhanced densification have been given, including the liquid phase sintering. Based on our recent study [15], however, a viscous flow mechanism has been identified to dominate the early-stage sintering of these metal oxides doped with small amounts of these TMOs. The authors believe that the Mn doping changes the early-stage sintering mechanism of ceria-based solid solutions to viscous flow. The viscous flow mechanism leads to a rapid densification rate at lower temperatures, which increases the contact area of particles in a compact solid. This will promote mass diffusivity of the matrix and thus enhance further densification as well as grain growth during subsequent sintering.

XRD measurements confirm that $Ce_{0.8}Gd_{0.2}O_{1.9}$, with and without Mn doping, has the fluorite structure; no new phase is found even for the sample with 5% Mn doping. It is important to clarify the solubility of Gd_2O_3 in CeO_2, because it is closely related to the ionic conductivity of Gd-doped ceria ceramics. A systematic study [16] was done on the isothermal solubility at 1600 °C for the Gd_2O_3-CeO_2 system ($0.05 \le Gd/Ce \le 0.4$); an optimal Gd content (~20 at%) was also found for achieving the maximum conductivity. In this study the effect of sintering temperature on the solubility of Gd_2O_3 in CeO_2, with and without TMOs as sintering aids, was carried out by measuring the lattice parameter from XRD patterns. The samples were held at each temperature for 5 h. Figure 5 shows the lattice parameter of undoped and Mn-doped ceria solid solutions versus sintering temperature. The lattice parameters increase with increasing temperature until a maximum is achieved at ~1600 °C for $Ce_{0.9}Gd_{0.1}O_{1.95}$ and $Ce_{0.8}Gd_{0.2}O_{1.9}$. Above 1600 °C, the lattice parameter keeps almost constant. This suggests that in order to ensure the dissolution of Gd_2O_3 into CeO_2, a sintering temperature of ~1600 °C is required in our case. However, this dissolution temperature can be remarkably reduced by the addition of some TMOs, such as Fe_2O_3, MnO_2, CoO or CuO. For example, as shown in Fig. 5 (curve c), temperatures of ~1450 °C can be observed for 0.5% Mn doping. By comparing the results in Figs. 1, 2, 3, 4, it is obvious that this is closely related to the remarkable reduction in sintering temperatures by adding the TMOs as sintering aids. Moreover, according to the study by Chen and Chen [21], the effect of severely undersized dopant ions, which leads to a fast migration of defects, takes effect in the materials with either fluorite (e.g., CeO_2) or C-type (e.g., Gd_2O_3) structures. This indicates that doping with these TMOs not only reduces sintering temperatures but also promotes the homogeneous distribution of Gd_2O_3 in CeO_2.

The ionic conductivity of $Ce_{0.8}Gd_{0.2}O_{2-\delta}$ with and without Mn addition was measured by a two-probe complex impedance analysis. The interpretation of

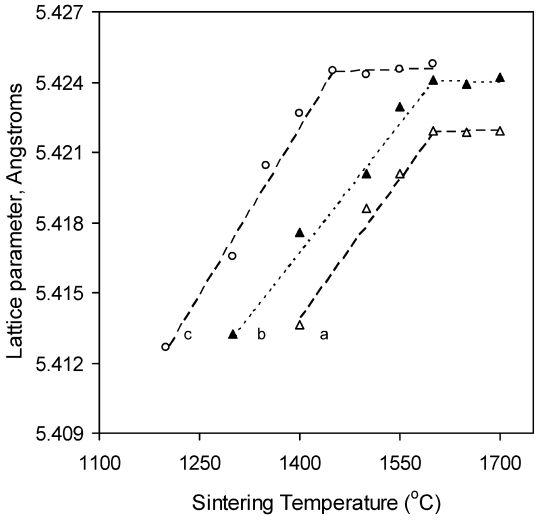

Fig. 5 Lattice parameter vs. sintering temperature for (*a*) $Ce_{0.9}Gd_{0.1}O_{1.95}$, (*b*) $Ce_{0.8}Gd_{0.2}O_{1.9}$ and (*c*) 1% Mn-doped $Ce_{0.8}Gd_{0.2}O_{1.9}$ ceramics

impedance data for polycrystalline materials, such as yttria-stabilized zirconia, has been well documented [22, 23]. In general, the a.c. impedance of an ionic conductor measured by a two-probe method contains contributions from the grain interior, grain boundaries and electrode/electrolyte interface, which can be reflected in a complex plane by three successive arcs, as shown in Fig. 6b. The frequency increases from the right to the left across a plot. The arc at the high-frequency end of the spectrum represents the grain-interior resistivity; the arc at the middle of the spectrum is a consequence of the grain-boundary effect; and the low-frequency arc is assigned to the electrode response. An idealized equivalent circuit for ceramic oxides corresponding to the impedance plot (Fig. 6b) is shown in Fig. 6a. In a practical case, however, not all these arcs can be observed, depending on the nature of the samples and testing conditions. For our case, three arcs can be identified clearly at a lower temperature (usually <250 °C). Figure 7 shows the impedance plots of samples with different Mn contents measured at 300 °C in air. This figure clearly shows that the addition of MnO_2 has a detrimental effect on grain boundary behavior. The quantitative change in grain interior and grain boundary conductivities can be obtained by fitting these impedance data using a software package, and the results are shown in Figs. 8, 9, 10.

Compared with the undoped $Ce_{0.8}Gd_{0.2}O_{2-\delta}$, Mn-doped samples exhibit a lower total conductivity (σ_t) (Fig. 10). This results mainly from an enlarged grain-boundary effect (σ_{gb}) in Mn-doped samples (Fig. 9), since Mn doping has little effect on grain interior conductivity (σ_{gi}) in Fig. 8. It is widely accepted that the predominant constituent of the grain boundary impurities in ceria-based solutions is SiO_2, and SiO_2 contamination results mainly from precursor chemicals and the sample preparation. An amorphous thin SiO_2 film will be formed between the grains during sintering, blocking the movement of oxygen ions through the grain boundary and leading to a lower conductivity. According to Steele [24], the grain boundary effect for clean $Ce_{0.9}Gd_{0.1}O_{2-\delta}$ cannot be detected above ~500 °C; however, it usually dominates the total conductivity up to ~1000 °C for impure $Ce_{0.9}Gd_{0.1}O_{2-\delta}$ samples. In our case, the exact content of SiO_2 in the samples used is unavailable at the present stage. Based on the results [25] from impedance spectroscopy, however, it can be deduced that the grain boundary effect dominates the total conductivity up to ~600 °C. This indicates that the Gd-doped ceria solid solution used in this study is an impure one. Moreover, as shown in Fig. 7, Mn doping enlarges remarkably the grain boundary effect of $Ce_{0.8}Gd_{0.2}O_{2-\delta}$ ceramics. This implies that Mn doping may change the viscosity and wetting nature of SiO_2, leading to a redistribution of SiO_2 along the grain boundary. Recent

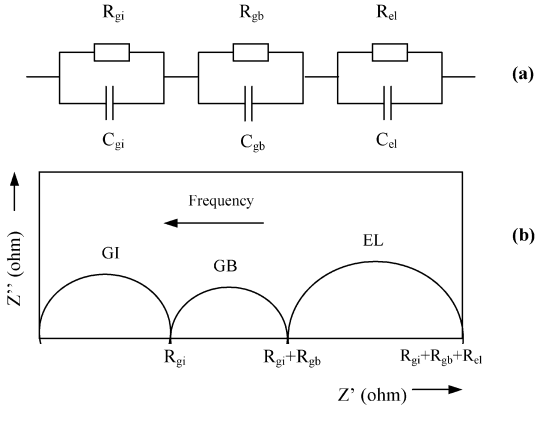

Fig. 6 An idealized equivalent circuit (**a**) and its corresponding impedance plot (**b**). R_{gi} and C_{gi}, R_{gb} and C_{gb}, and R_{el} and C_{el} represent resistances and capacitances for grain interior, grain boundary, and electrode process, respectively

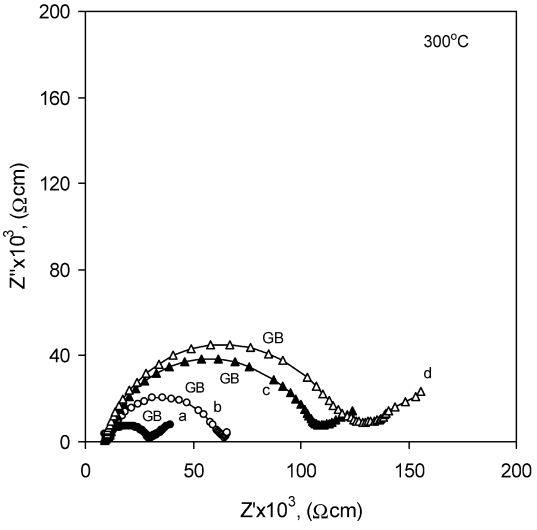

Fig. 7 Impedance plot measured at 300 °C for (*a*) 0% Mn, (*b*) 0.25% Mn, (*c*) 0.5% Mn and (*d*) 1% Mn-doped $Ce_{0.8}Gd_{0.2}O_{1.9}$ ceramics; GB stands for the grain boundary effect

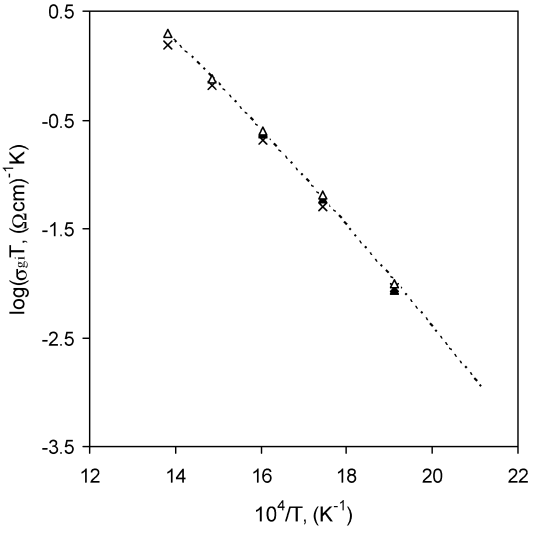

Fig. 8 Arrhenius plots of grain interior conductivity of 0% Mn- (*dashed line*), 0.25% Mn- (*open triangles*), 0.5% Mn- (*filled triangles*) and 1% Mn-doped (*crosses*) $Ce_{0.8}Gd_{0.2}O_{1.9}$ ceramics

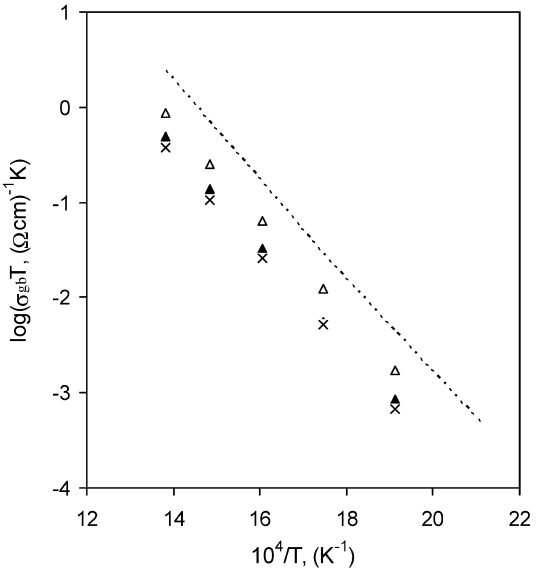

Fig. 9 Arrhenius plots of grain boundary conductivity of 0% Mn- (*dashed line*), 0.25% Mn- (*open triangles*), 0.5% Mn- (*filled triangles*) and 1% Mn-doped (*crosses*) $Ce_{0.8}Gd_{0.2}O_{1.9}$ ceramics

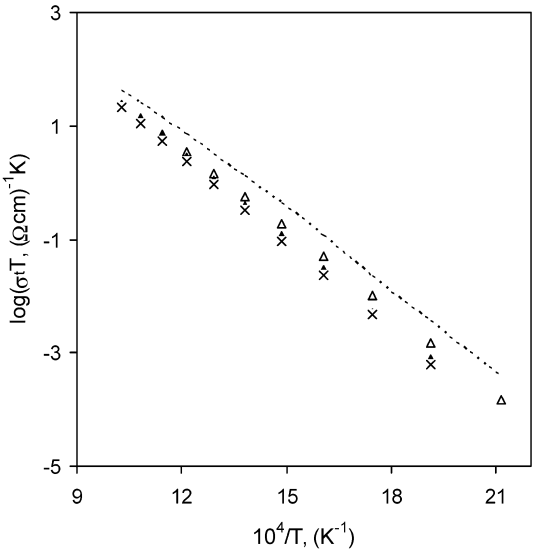

Fig. 10 Arrhenius plots of total conductivity of 0% Mn- (*dashed line*), 0.25% Mn- (*open triangles*), 0.5% Mn- (*filled triangles*) and 1% Mn-doped (*crosses*) $Ce_{0.8}Gd_{0.2}O_{1.9}$ ceramics

Table 1 Ionic conductivities[a] and activation energies of undoped and Mn-doped $Ce_{0.8}Gd_{0.2}O_{2-\delta}$

Composition	E_{gi} (eV)	E_{gb} (eV)	E_t (eV)	σ_{gi} $(\Omega\ cm)^{-1}$	σ_{gb} $(\Omega\ cm)^{-1}$	σ_t $(\Omega\ cm)^{-1}$
0% Mn-doped $Ce_{0.8}Gd_{0.2}O_{2-\delta}$	0.86	1.01	0.94	1.15×10^{-3}	1.02×10^{-3}	$1.74\times10_{-3}$
0.25% Mn-doped $Ce_{0.8}Gd_{0.2}O_{2-\delta}$	0.84	1.01	0.95	1.16×10^{-3}	4.1×10^{-4}	3.04×10^{-4}
0.5% Mn-doped $Ce_{0.8}Gd_{0.2}O_{2-\delta}$	0.87	1.04	1.01	1.14×10^{-3}	2.0×10^{-4}	1.65×10^{-4}
1% Mn-doped $Ce_{0.8}Gd_{0.2}O_{2-\delta}$	0.86	1.03	1.01	1.14×10^{-3}	1.35×10^{-4}	1.2×10^{-4}

[a]Conductivities (σ_{gi}, σ_{gb} and σ_t) were measured at 300 °C

work by Appel and Bonanos [26] showed that the co-doping of SiO_2 and MnO_2 leads to a much more pronounced grain boundary effect in yttria-stabilized zirconia than only SiO_2 doping. Their TEM analysis revealed that Mn doping promoted the propagation of SiO_2 along the grain boundary. This is attributed to the formation of a liquid phase between SiO_2 and Mn oxides at lower temperatures (< 1350 °C) [27]. By analogy, the enlarged grain boundary behavior in Mn-doped $Ce_{0.8}Gd_{0.2}O_{2-\delta}$ (Fig. 8) is closely related to Mn doping causing the formation of a Si-containing liquid phase and propagation of this Si-containing phase along the grain boundary. However, this Si-containing film does not enclose all the grains. This can be deduced from the values of the activation energy for grain boundary conduction in Table 1. In the case of the experimental testing errors, it is reasonable to consider that these values for undoped and doped samples are almost the same, indicating that oxygen ions cross the grain boundary through the "clean" grain-to-grain contact (i.e., intrinsic), instead of a grain boundary phase. Otherwise, the values of the activation energy for grain boundary conduction will change with the composition of the grain boundary phase. As a matter of fact, most of the literature reports [28, 29, 30] revealed that Si-containing glass phases were enriched mainly in the triple junction points and along some of the grain boundaries, and only in a few cases enclosed all the grains.

In the case of the fact that Mn-containing perovskite compounds such as $La_{0.8}Sr_{0.2}MnO_{3-\delta}$ are widely used as electrodes for SOFCs, it should be pointed out that optimization of the electrode fabrication conditions is needed since Mn will diffuse from the electrode side to the electrolyte to form a low-conductivity layer at the electrode/electrolyte interface.

References

1. Nakamura A, Wagner JB Jr (1980) J Electrochem Soc 127:2325
2. Verkerk J, Middelhuis BJ, Burgraaf AJ (1982) Solid State Ionics 6:159
3. Inda H, Tagana H (1996) Solid State Ionics 83:1
4. Atkinson A (1997) Solid State Ionics 95:249
5. Steele BCH (2000) Solid State Ionics 129:95
6. Kudo T, Obayashi H (1975) J Electrochem Soc 122:142
7. Yahiro H, Eguchi K, Arai H (1998) J Electrochem Soc 135:2077
8. Huang K, Feng M, Goodenough JB (1998) J Am Ceram Soc 81:357

9. Mogensen M, Lindegaard T, Hansen UR, Mogensen G (1994) J Electrochem Soc 141:2122
10. Kleinlogel C, Gauckler LJ (2000) Solid State Ionics 135:567
11. Kleinlogel C, Gauckler LJ (1999) Proceedings of SOFC VI. (The Electrochemical Society proceedings series, vol 99-19) The Electrochemical Society, Pennington, NJ, pp
12. Lewis GS, Atkinson A, Steele BCH (2000) 4th European SOFC Forum, vol. 2
13. Kovalevskii AV, Kharton VV, Naumovich EN (1996) Inorg Mater 32:1230
14. Zhang TS, Hing P, Huang H, Kilner J (2001) Mater Sci Eng B 83:235
15. Zhang TS, Hing P, Huang H, Kilner J (2002) J Mater Sci 37:997
16. Zhang TS, Hing P, Huang H, Kilner J (2002) Solid State Ionics 148:567
17. Bonnet JP, Dolet N, Heintz JM (1996) J Eur Ceram Soc 16:1163
18. Varela JA (1996) J Am Ceram Soc 79:789
19. Kim DW, Kim TG, Hong KS (1999) Mater Res Bull 34:771
20. Sumita S, Entbowen H (1987) Ceramic transactions: ceramic powder science II
21. Chen PL, Chen IW (1996) J Am Ceram Soc 79:1793
22. Bauerle JE (1969) J Phys Chem Solids 30:2657
23. Macdonald JR (1987) Impedance spectroscopy, emphasizing solid materials and systems. Wiley, New York
24. Steele BCH (2000) Solid State Ionics 129:95
25. Zhang TS, Hing P, Huang H, Kilner J (2002) Solid State Ionics (in press)
26. Appel CC, Bonanos N (1999) J Eur Ceram Soc 19:847
27. Muan A (1959) Am J Sci 257:297
28. Gerhardt R, Nowick AS, Mochel ME, Dumler I (1986) J Am Ceram Soc 69:649
29. Stoto T, Nauer M, Larry C (1991) J Am Ceram Soc 74:2615
30. Badwal SPS, Ciacchi FT, Hannink RHG (1990) Solid State Ionics 40/41:882